

Numerical Studies of the Asymptotic Behavior of a Reaction-Diffusion System with a Fast Reaction

Yushu Yang, Michael Muscedere, and Matthias K. Gobbert

Department of Mathematics and Statistics, University of Maryland, Baltimore County

1000 Hilltop Circle, Baltimore, MD 21250

{yushu1,mmusce1,gobbert}@math.umbc.edu

Abstract. A model system of reaction-diffusion equations exhibiting a fast reaction is studied with an initial condition defining three interfaces between regions of dominance of two main reactants within the spatial domain. Two cases varying the reactant coefficient of the model problem are studied, the second case using reactant coefficient three orders of magnitude larger than the first. A numerical method consisting of spatial discretization by finite differences in space and a time discretization employing Numerical Differentiation Formulas is used to obtain numerical solutions for both cases. Comparing the numerical interface solutions between the two cases shows that the asymptotic limit of the model problem has been nearly approached for both reaction coefficients considered. Therefore, the qualitative features of the internal reactant boundaries can be reliably studied using the smaller reaction coefficient, saving substantial computation time. This report also includes a systematic study of several numerical parameters including the absolute and relative ODE tolerances that guarantee the efficiency and reliability of the numerical solutions used to draw the conclusions about the model solutions.

Keywords. Reaction-diffusion equations, chemical kinetics, method of lines, numerical differentiation formulas, stiff system.

AMS subject classifications (2000). 35K57, 65L99, 65M06, 65M20, 80A30.

1 Introduction

This note considers the diffusive flow of chemical species inside a membrane that separates two reservoirs with unlimited supplies of the reactants A and B, respectively, that participate in the chemical reaction $2A + B \rightarrow (*)$. The evolution of the concentrations of the species can be modeled by a system of transient reaction-diffusion equations. This model becomes mathematically intriguing as well as numerically challenging if one considers a particular reaction pathway comprising two reactions with widely varying rate coefficients [5]: Molecules of A and B combine in a first, ‘fast’ reaction to produce an intermediate C, while a second, ‘slow’ reaction combines A and C to form the product (*), which is not explicitly tracked in the model. This reaction pathway is expressed by



in which the reaction coefficients λ and μ are scaled so that $\lambda \gg \mu = 1$.

For the steady-state of this problem, analytical results in [1, 2] prove that the reaction rate of the fast reaction has an internal layer of width $O(\varepsilon)$ and height $O(1/\varepsilon)$ with the scaling $\varepsilon = \lambda^{-1/3}$ in terms of the reaction coefficient of the ‘fast’ reaction $\lambda \gg 1$. This result is based on asymptotic analysis in the limit $\lambda \rightarrow \infty$. But in numerical simulations, the value λ needs to be finite. In past studies [4, 5], we considered the values $\lambda = 10^3$, 10^6 , and 10^9 for numerical studies of the steady-state problem, as these give rise to ‘nice’ values for the scaling of $\varepsilon = 0.1$, 0.01 , and 0.001 , respectively. However, most transient studies used $\lambda = 10^6$. This value was chosen so that a numerical mesh in space could comply with the requirement that its mesh spacing Δx be an order of magnitude less than ε , while not making the numerical solution too

costly to handle. Specifically, if the domain $[0, 1]$ is discretized using N nodes, then the mesh spacing is $\Delta x = 1/(N - 1)$. With $N = 2^{10} + 1 = 1025$, then $\Delta x = 1/1024 \approx 0.001$, giving several mesh points within the scaling width $\varepsilon = 0.01$ for $\lambda = 10^6$. Using the same requirement led to the use of $N = 2^{13} + 1 = 8193$ mesh points for the studies performed for $\lambda = 10^9$. However, extensive studies with this resolution are costly numerically, due to the large number of time steps required.

Therefore, before proceeding with further studies, it is important to determine the optimal numerical parameters, that is, parameters that ensure a reliable solution but with possibly fewer spatial points and larger time steps. This question needs to be analyzed for each value of λ individually. But even more fundamentally, we can then combine the results for several λ values to determine at which value the process is in its asymptotic limit. Concretely, simulations with $\lambda = 10^6$ are relatively inexpensive, while simulations with $\lambda = 10^9$ are relatively costly. If careful reference studies with both values turn out to give nearly identical results for the relevant quantities of interest, then we can conclude that the process is already in its asymptotic limit for $\lambda = 10^6$ and that therefore studies using this value suffice to study the behavior of the process. It will turn out below that we can answer this question in the affirmative. This result is the main conclusion of this note, explained at the end of Section 2 after introducing the model and its parameters. Section 3 then summarizes the numerical method used, after which Sections 4 and 5 present careful studies of the crucial numerical simulation parameters for $\lambda = 10^6$ and 10^9 , respectively, that give us confidence in the results for each value of λ .

2 The Model

The chemical reactions in (1.1) take place inside a membrane that is thin compared to the directions normal to it. Thus, it is reasonable to use a one-dimensional spatial domain with variable x , scaled so that $x \in \Omega := (0, 1)$. In time, we compute from the initial time 0 to the final time t_{fin} , which is chosen such that the solution has reached its steady state. We denote the concentrations of the chemical species A, B, C by functions $u(x, t)$, $v(x, t)$, $w(x, t)$, respectively, the reaction-diffusion system reads

$$\left. \begin{aligned} u_t &= u_{xx} - \lambda uv - uw, \\ v_t &= v_{xx} - \lambda uv, \\ w_t &= w_{xx} + \lambda uv - uw, \end{aligned} \right\} \quad \text{for } x \in (0, 1) \text{ and } 0 < t \leq t_{\text{fin}}. \quad (2.1)$$

The boundary conditions are a combination of Dirichlet and Neumann boundary conditions given by

$$\begin{aligned} u &= \alpha, & v_x &= 0, & w_x &= 0 & \text{at } x = 0, \\ u_x &= 0, & v &= \beta, & w_x &= 0 & \text{at } x = 1. \end{aligned} \quad (2.2)$$

The problem statement of this initial-boundary value problem is completed by specifying the non-negative initial concentrations

$$u(x, 0) = u_{\text{ini}}(x), \quad v(x, 0) = v_{\text{ini}}(x), \quad w(x, 0) = w_{\text{ini}}(x) \quad \text{for } x \in (0, 1) \text{ at } t = 0. \quad (2.3)$$

We assume that the boundary and initial data are posed consistently; i.e., $u_{\text{ini}}(0) = \alpha$, and $v_{\text{ini}}(1) = \beta$.

Because the first chemical reaction is much faster than the second one, rapid consumption of A and B to form C is expected at all spatial points x where A and B co-exist, leaving only one of them present with a positive concentration after an initial transient. Inside the regions dominated either by A or by B, the reaction rate of the fast reaction $q := \lambda uv$ will then become 0. However at the interfaces between the regions, where positive concentrations of A and B make contact due to diffusion, q will be non-zero; in fact, q will be large due to the large coefficient $\lambda \gg 1$. The analytical results in [1, 2] prove that at its steady-state limit the reaction rate of the fast reaction q has one internal layer at a point $0 < x^* < 1$ of width $O(\varepsilon)$ and height $O(1/\varepsilon)$ with the scaling $\varepsilon = \lambda^{-1/3}$. Because initial conditions to the transient problem can have the internal layer at a different position than x^* or can have multiple internal layers, it is interesting to investigate the evolution of the internal layers and their coalescence to the single layer present

at steady state. See [4, 5] for studies of the evolution of these internal layers for several representative initial conditions.

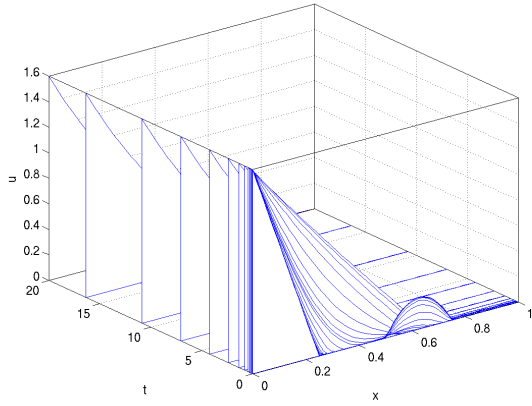
To select a transient problem for testing that has the stationary solution just described and an interesting transient behavior, we select an initial condition with three interfaces specified by the initial condition functions for (2.3) chosen as

$$\begin{aligned}
 u_{\text{ini}}(x) &= \begin{cases} 4(0.25 - x) \alpha, & 0.00 \leq x \leq 0.25, \\ 0, & 0.25 < x < 0.50, \\ 64(0.50 - x)(x - 0.75) \gamma, & 0.50 \leq x \leq 0.75, \\ 0, & 0.75 < x \leq 1.00, \end{cases} \\
 v_{\text{ini}}(x) &= \begin{cases} 0, & 0.00 \leq x < 0.25, \\ 64(0.25 - x)(x - 0.50) \delta, & 0.25 \leq x \leq 0.50, \\ 0, & 0.50 < x < 0.75, \\ 4(x - 0.75) \beta, & 0.75 \leq x \leq 1.00, \end{cases} \\
 w_{\text{ini}}(x) &\equiv 0.
 \end{aligned} \tag{2.4}$$

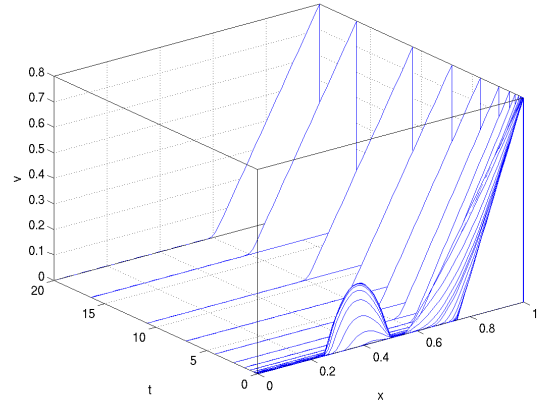
The parameters α and β come from the boundary conditions (2.2), and their use in (2.4) guarantees that the initial conditions are consistent with the boundary conditions; therefore there are no boundary layers in the solutions, and we can focus our attention on the internal layers. The design in (2.4) produces linear functions in u and v at their respective Dirichlet boundary conditions and one quadratic hump for u and v each in the interior of the spatial domain, such that u and v are not non-zero simultaneously. Thus, for the parameters that affect the steady state solution, we pick $\alpha = 1.6$, and $\beta = 0.8$. For the values γ and δ that control the height of the humps of u and v in (2.4), we choose $\gamma = \delta = 0.25$. For the final time, we select $t_{\text{fin}} = 20$; experiments show that this time is sufficient to reach the steady state solution using the criterion that the location x^* of the internal layer at steady state is approximated up to the resolution achievable by the spatial discretization.

Simulation results for the model with reaction coefficient $\lambda = 10^6$ are shown in Figure 1. Figures 1 (a), (b), and (c) show waterfall plots of the concentrations $u(x, t)$, $v(x, t)$, and $w(x, t)$, respectively, vs. (x, t) . As seen at time zero in the waterfall plots of Figures 1 (a) and (b), u and v are initially non-zero in complimentary regions in the interior of $\Omega = (0, 1)$. Figure 1 (c) shows the third species w , which is an intermediate of the reaction pathway with two reactions. It grows from zero initially to a positive steady-state value, reflecting the fact that the slower second reaction cannot consume it faster than it is created. Figure 1 (d) shows the plot of the reaction rate $q = \lambda uv$ vs. (x, t) . We observe that q is zero in most of the domain, as either u or v are zero there. But q is large at the interfaces of the regions where either u or v dominate, as a result of the diffusion that moves u and v from their regions of dominance and brings them in contact at the interfaces of these regions. Notice that w is thus only created at the localized interfaces, but is then present throughout Ω , as seen in Figure 1 (c), solely due to its diffusion. We also see in Figure 1 (d), for larger time that only one spike exists for q compared to three at the initial time. The waterfall plot in Figure 1 (d) provides information about the location of the interface between regions of dominance by u or v only at selected points in time. To visualize the interface and its movement over time more clearly, Figure 1 (e) plots its location for all time steps in the numerical study $0 \leq t \leq 20$. We can see that the interface moves slowly and smoothly to its steady-state value of $x^* \approx 0.6$. To get a clearer picture of the interface movement for small times, Figure 1 (f) zooms in on the time span $0 \leq t \leq 0.1$. This confirms that the three interfaces present initially are located at $x = 0.25, 0.50$, and 0.75 . Figure 1 (f) shows how quickly the three interfaces coalesce to one. This makes it clear that one of the most interesting features of this problem is the behavior of the concentration interfaces between regions dominated by either u or v , which is why we refer to this problem as the interface problem.

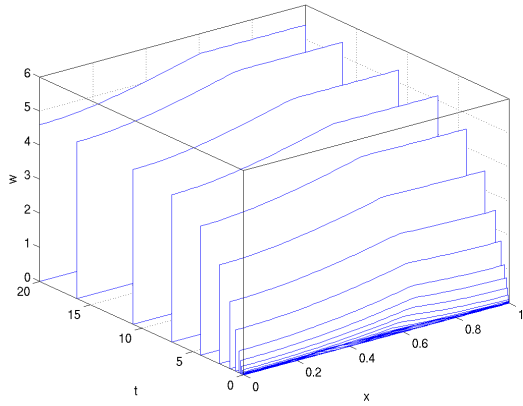
Figure 2 shows the simulation results for the model with reaction coefficient $\lambda = 10^9$, arranged analogously to Figure 1. Notice in Figure 2 (d), the reaction rate spikes are now higher and narrower than seen for the reaction coefficient $\lambda = 10^6$. This is expected given that the value $\lambda = 10^9$ results in a scaling of width $\varepsilon = 0.001$ with height $1/\varepsilon = 1,000$, compared with width $\varepsilon = 0.01$ and height $1/\varepsilon = 100$ for $\lambda = 10^6$.



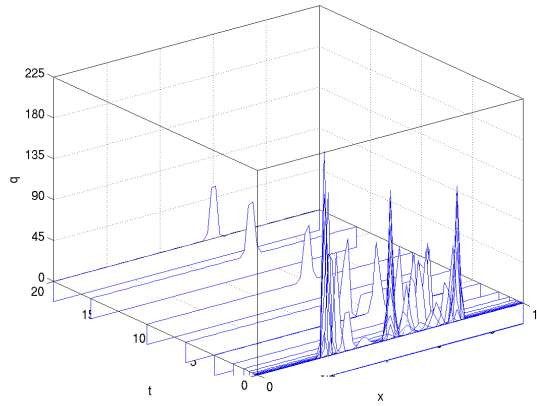
(a) u vs. (x, t)



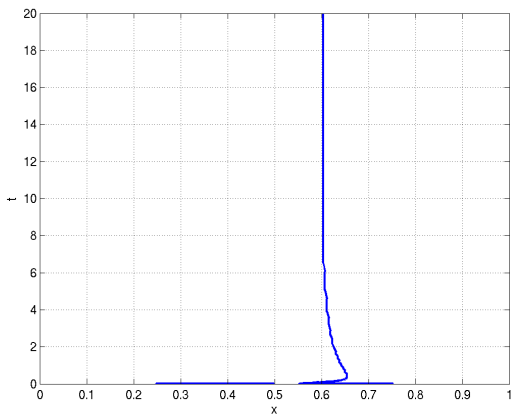
(b) v vs. (x, t)



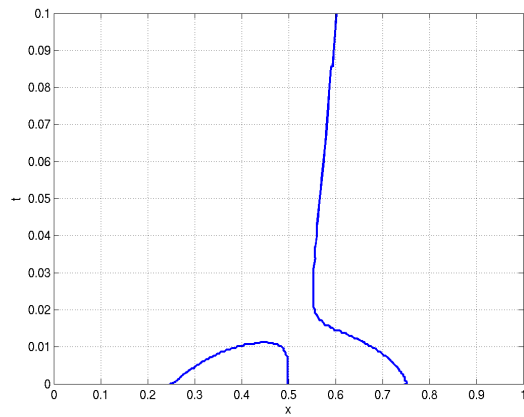
(c) w vs. (x, t)



(d) $q = \lambda uv$ vs. (x, t)



(e) interface vs. (x, t)



(f) zoomed interface vs. (x, t)

Figure 1: Simulation results for the interface problem with $\lambda = 10^6$. (a), (b), (c) Concentrations u , v , w vs. (x, t) , respectively. (d) Reaction rate $q = \lambda uv$ vs. (x, t) . (e) Concentration interface in the (x, t) -plane for the entire time span $0 \leq t \leq 20$. (f) Concentration interface in the (x, t) -plane zoomed into the time span $0 \leq t \leq 0.1$. These studies used $N = 2^{10} + 1$ mesh points, and absolute and relative ODE tolerances of 10^{-4} both.

Notice that on the scale of Figure 2 (d) we cannot tell the height of q at latter times t when approaching the steady-state. Therefore, Figure 2 (e) and (f) are again designed to provide the detailed insight into the evolution of the reactant interfaces. Comparing their plots in Figures 1 and 2, we observe that they behave very similarly.

Motivated by the the similarity of the plots of the concentration interfaces shown in Figures 1 and 2, Figure 3 shows overlays of these interfaces for both reaction coefficients $\lambda = 10^6$ and $\lambda = 10^9$ in the (x, t) -plane. For each value of λ , results from two numerical studies are shown to ensure reliability of the results. The top four plots in the figure overlay the cases in progressively decreasing time spans. The left bottom plot shows the movement of the left portion of the interface zoomed into $0.3 \leq x \leq 0.5$ and $0.005 \leq t \leq 0.014$. The right bottom plot of Figure 3 shows the movement of the right portion of the interface zoomed into $0.5 \leq x \leq 0.7$ and $0.05 \leq t \leq 0.95$. We see in Figure 3 that the computed solution representing the motion of the concentration interfaces for $\lambda = 10^6$ and $\lambda = 10^9$ are very close in every time span and zoom view. This suggests that the solution to the problem is near the asymptotic limit ($\lambda \rightarrow \infty$) already for the value $\lambda = 10^6$. In [1], it was shown analytically for the stationary problem that the error between the limit solution and a solution for finite λ is uniformly on the order of $\varepsilon = \lambda^{-1/3}$. The present computational results show that the same estimate appears to hold for the transient problem. Therefore, we conclude that the features of the interface movement can be reliably studied using $\lambda = 10^6$. We will see in Sections 4 and 5 that the maximum computation time for the $\lambda = 10^6$ cases used in Figure 3 is on the order of 17 seconds, while already the minimum computation time for the $\lambda = 10^9$ cases is 127 seconds. This difference in computation time demonstrates the importance of the conclusion for future parameter studies for this problem.

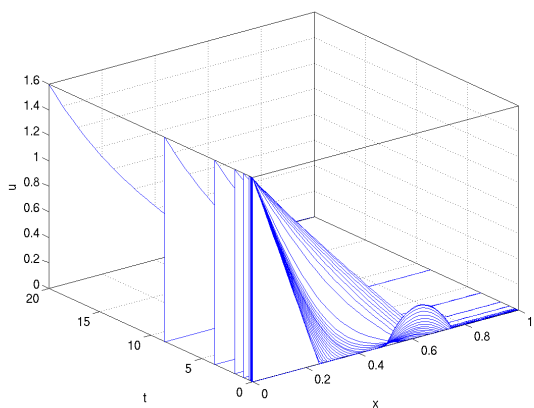
3 Numerical Method

The interface problem (2.1)–(2.3) is discretized by the finite difference method within a method of lines approach. We define a uniform spatial mesh with N nodes across the spatial domain $\bar{\Omega} = [0, 1]$ with mesh spacing $\Delta x = 1/(N - 1)$ by $x_j = (j - 1) \Delta x$ for $j = 1, \dots, N$. Then, let $u_j(t)$, $v_j(t)$, $w_j(t)$ denote approximations to $u(x_j, t)$, $v(x_j, t)$, $w(x_j, t)$, respectively. At each node x_j , $j = 1, \dots, N$, a finite difference discretizes the spatial derivatives, still leaving the time dependence of all quantities. To write this system of ordinary differential equations (ODEs) for functions $u_j(t)$, $v_j(t)$, $w_j(t)$ in vector form, define the vector functions $U(t) := [u_1, \dots, u_N]^T$, $V(t) := [v_1, \dots, v_N]^T$, and $W(t) := [w_1, \dots, w_N]^T$ with N components. Combining them moreover in the vector function $y(t) := [U^T, V^T, W^T]^T$ with $3N$ components allows then to collect the problem to be simulated in the form of an ODE system in standard form

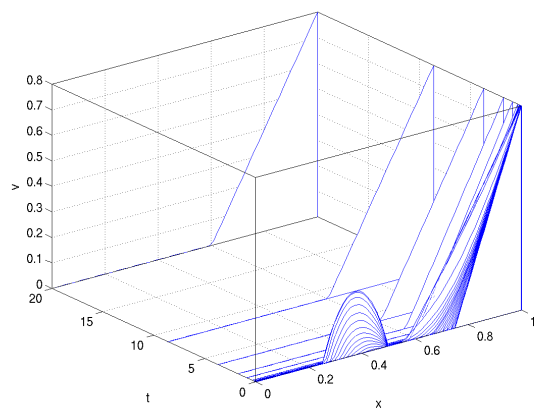
$$\frac{dy}{dt} = f(t, y), \quad 0 < t \leq t_{\text{fin}}, \quad y(0) = y_{\text{ini}}, \quad (3.1)$$

Appendix A derives this system in detail and explains the choices in the finite difference discretization, in particular, how the boundary conditions are handled in this context.

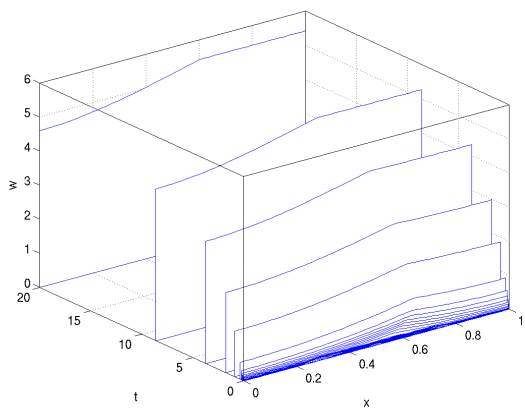
Since the problem has significant transients in time, it is vital for efficient simulations that the ODE solver vary its time steps to be small during the transient for accuracy and to be large outside of the transients for efficiency. To this end, we use Matlab’s `ode15s` function, which is an implementation of the Numerical Differentiation Formulas (NDF k) [3], a generalization of the well-known Backward Differentiation Formulas (BDF k). Both methods are families of variable method order $1 \leq k \leq 5$ and suitable for the solution of stiff ODE systems arising from method of lines discretizations of reaction-diffusion equations. ODE methods for stiff systems must necessarily use implicit time discretizations. Since the original problem (2.1) involves non-linear terms, this implicit time discretization results in a system of non-linear equations, which is solved at every time step by the Newton method. The linear solver at every Newton step is Gaussian elimination (with LU factorization retained until the system matrix changes), which is efficient for a PDE problem in one spatial dimension. The implementation in `ode15s` includes sophisticated automatic method order and step size selection, based on estimating the local error of the computed at



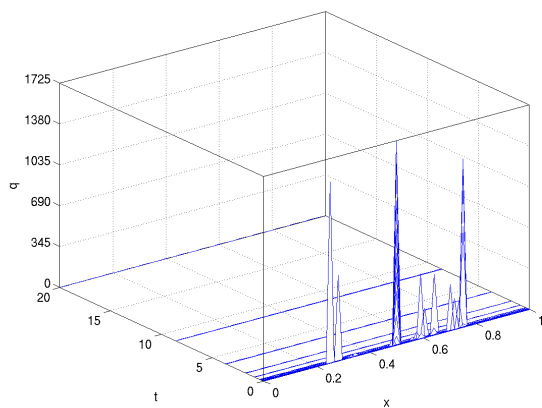
(a) u vs. (x, t)



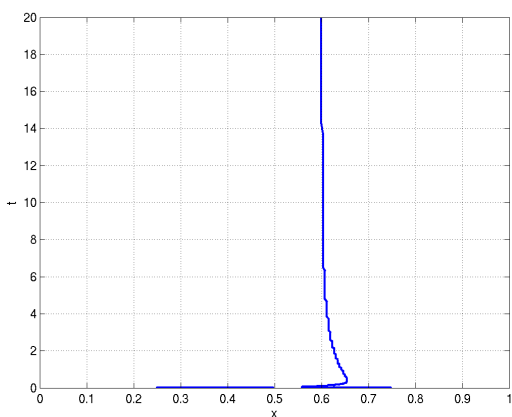
(b) v vs. (x, t)



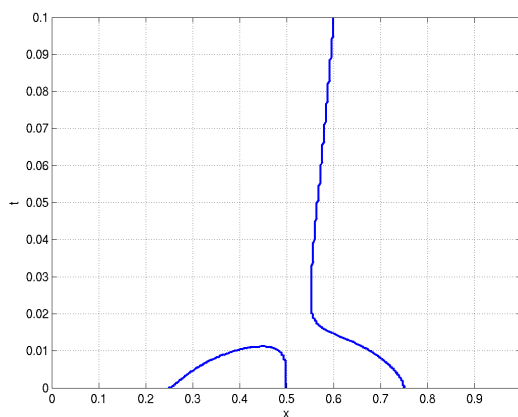
(c) w vs. (x, t)



(d) $q = \lambda uv$ vs. (x, t)



(e) interface vs. (x, t)



(f) zoomed interface vs. (x, t)

Figure 2: Simulation results for the interface problem with $\lambda = 10^9$. (a), (b), (c) Concentrations u , v , w vs. (x, t) , respectively. (d) Reaction rate $q = \lambda uv$ vs. (x, t) . (e) Concentration interface in the (x, t) -plane for the entire time span $0 \leq t \leq 20$. (f) Concentration interface in the (x, t) -plane zoomed into the time span $0 \leq t \leq 0.1$. These studies used $N = 2^{10} + 1$ mesh points, and absolute and relative ODE tolerances of 10^{-8} and 10^{-6} , respectively.

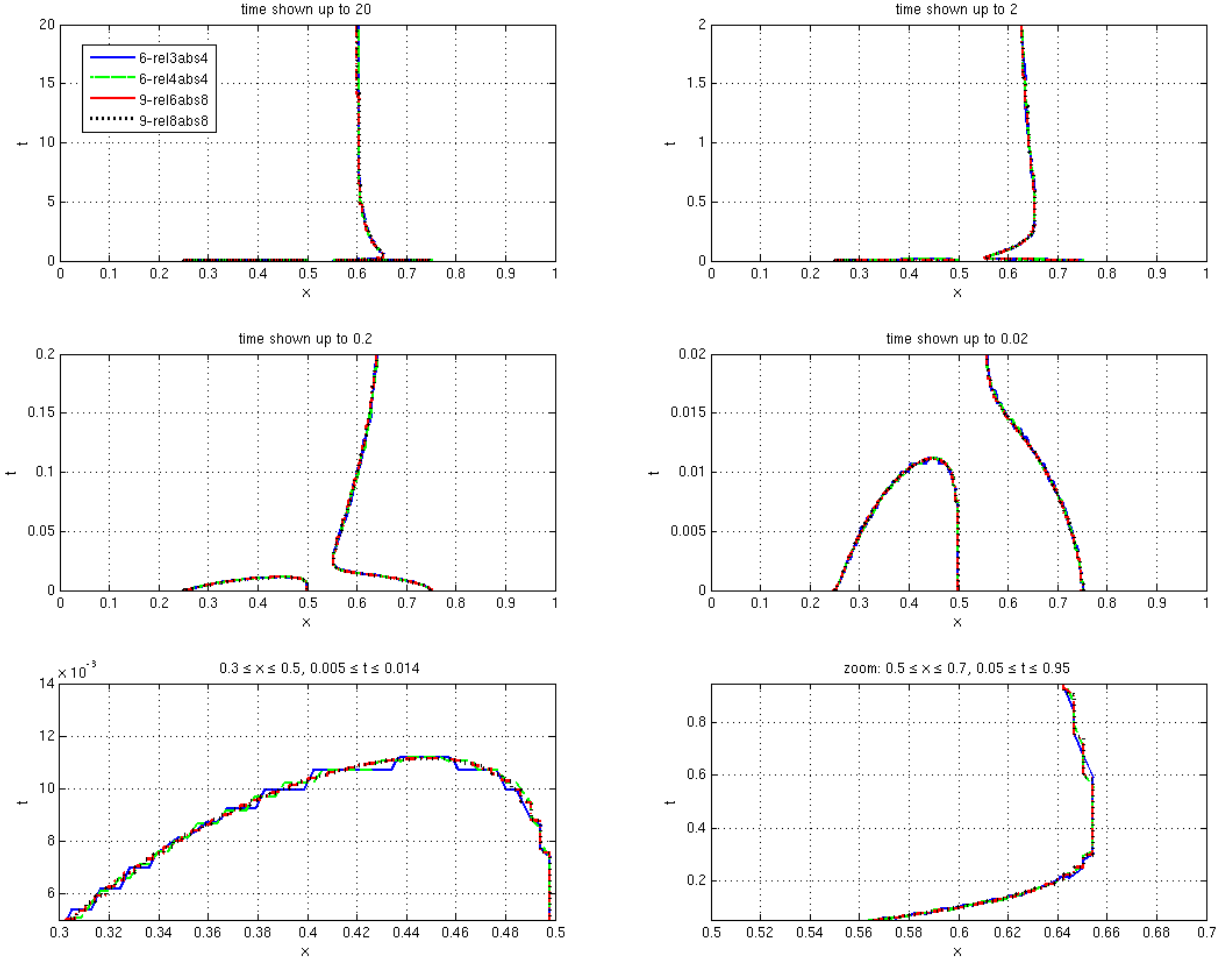


Figure 3: Simulation results of the concentration interface for both reaction coefficients $\lambda = 10^6$ and $\lambda = 10^9$ in the (x, t) -plane. The top four plots overlay these cases for comparison in progressively decreasing time spans. The left bottom plot shows the movement of the left portion of the interface zoomed into $0.3 \leq x \leq 0.5$ and $0.005 \leq t \leq 0.014$. The right bottom plot shows the movement of the right portion of the interface zoomed into $0.5 \leq x \leq 0.7$ and $0.05 \leq t \leq 0.95$. A mesh size of $N = 2^{10} + 1$ is used for both values of λ . The data shown for $\lambda = 10^6$ used an absolute ODE tolerance of 10^{-4} and relative tolerances of 10^{-3} and 10^{-4} . The data shown for $\lambda = 10^9$ used an absolute ODE tolerance of 10^{-8} and relative tolerances 10^{-6} and 10^{-8} .

every time step [3]. The user has control over the absolute and relative tolerance demanded of this error estimator, where tighter tolerances are expected to result in higher accuracy of the solution at the expense of smaller time steps and more costly simulations. Therefore, the user has an interest in not selecting the tolerances unnecessarily tight, but rather we wish to find the coarsest tolerances possible for efficiency that still give reliable, accurate numerical results. Thus, careful studies were performed to analyze the behavior of the numerical method and the reliability of the solution, which are presented in the following two sections for $\lambda = 10^6$ and $\lambda = 10^9$, respectively.

4 Numerical Results for $\lambda = 10^6$

Table 1 shows the `ode15s` efficiency statistics for the case of $\lambda = 10^6$. The number of ODE steps (S), number of Jacobian evaluations (P), number of LU decompositions (D), and computation time (T) in seconds are reported across relative (rel) and absolute (abs) ODE tolerances for each mesh size $N = 2^n + 1$ for $n = 9, 10, 11, 12$. The values of both absolute and relative tolerances used in the study are 10^{-1} , 10^{-2} , 10^{-3} and 10^{-4} for each mesh size N . Table 1 uses an **(F)** to identify instances when the ODE solver stops with an error short of the final time $t_{\text{fin}} = 20$ since the time step size cannot be decreased below the minimum allowable value. An **(F)** in the “rel” column indicates failure for that particular value of relative tolerance across every absolute tolerance value. We start by observing that ODE solver breaks down before reaching the final time for the coarsest relative tolerances 10^{-1} and 10^{-2} . But Table 1 also shows that the numerical method begins to succeed for relative tolerance values tighter than or equal to 10^{-3} for all the values of the absolute tolerance considered. Considering elapsed time T , we see it increases for larger N , but no pattern emerges as we vary the relative tolerances. However as we tighten the absolute tolerances, computation time does increase until we reach 10^{-3} and then it remains unchanged for 10^{-4} . We note that the maximum computation time in Table 1 for the $\lambda = 10^6$ cases $N = 2^{10} + 1$ with absolute tolerance 10^{-4} and relative tolerances 10^{-3} and 10^{-4} , that were used for comparing the interface accuracy in Figure 3, is 17 seconds.

Considering only the convergent cases, the ODE solver needs more steps S to converge for tighter relative tolerances. We also see a dependence between absolute and relative ODE tolerances when considering the number of ODE step S required for convergence. Notice that when the relative tolerance is 10^{-3} , the number of ODE steps seems to stabilize at a fixed value for absolute tolerance equal to 10^{-2} or tighter, while for relative tolerance 10^{-4} , S stabilizes for absolute tolerance 10^{-3} and tighter. We also observe that the number of Jacobian evaluations and LU decompositions both increase modestly as the relative tolerance decreases from 10^{-3} to 10^{-4} .

Keeping the relative tolerance constant, we now check the accuracy of the solution by considering plots of the concentration interface motion as reference. Figure 4 shows plots of the concentration interface in the (x, t) -plane for reaction coefficient $\lambda = 10^6$ using mesh size $N = 2^{10} + 1$. The data corresponding to $\lambda = 10^6$ was collected with relative tolerance of 10^{-4} while the absolute tolerances varied within the set of values 10^{-1} , 10^{-2} , 10^{-3} and 10^{-4} . The top four plots overlay these cases for comparison in progressively decreasing time spans. The left bottom plot shows the movement of the left portion of the interface zoomed into $0.3 \leq x \leq 0.5$ and $0.005 \leq t \leq 0.014$. The right bottom plot shows the movement of the right portion of the interface zoomed into $0.5 \leq x \leq 0.7$ and $0.05 \leq t \leq 0.95$. We observe the results for each absolute tolerance value track closely with each other. Therefore, we see no significant change in accuracy.

Conversely, we check the interface plots for accuracy in the solution by holding the absolute tolerance constant. Figure 5 shows plots analogous to Figure 4 but now holding the absolute tolerance constant at 10^{-4} and varying the relative tolerance values 10^{-1} , 10^{-2} , 10^{-3} and 10^{-4} . Note the top left plot of Figure 4 shows the simulation does not reach the prescribed final time $t_{\text{fin}} = 20$ for relative tolerances 10^{-1} (blue solid line) and 10^{-2} (green dashed line) as was pointed out while discussing the results of Table 1. Rather, Figure 4 shows the simulation terminates near time 0.12 as seen in the middle right plot for relative tolerance 10^{-1} . Furthermore, in the top left plot of the figure the simulation for relative tolerance 10^{-2} terminates near time 5.5. For the remaining two convergent cases, the overlay plots show that the results

Table 1: Table of `ode15s` efficiency statistics for $\lambda = 10^6$. The number of ODE steps (S), number of Jacobian evaluations (P), number of LU decompositions (D) and computation time (T) in seconds are reported across absolute tolerances (abs) and relative (rel) values for each mesh size $N = 2^n + 1$ for $n = 9, 10, 11, 12$. An **(F)** in the (rel) column indicates failure for that particular value of relative tolerance across every absolute tolerance value.

(a) $N = 2^9 + 1$																	
rel \ abs		10^{-1}				10^{-2}				10^{-3}				10^{-4}			
		S	P	D	T												
10^{-1}	(F)	138	48	129	11	138	48	129	12	138	48	129	11	138	48	129	11
10^{-2}	(F)	176	63	160	15	176	63	160	15	176	63	160	15	176	63	160	15
10^{-3}		94	27	62	6	111	36	64	8	111	36	64	8	111	36	64	8
10^{-4}		94	27	62	10	125	35	65	9	155	33	66	10	155	33	66	10
(b) $N = 2^{10} + 1$																	
rel \ abs		10^{-1}				10^{-2}				10^{-3}				10^{-4}			
		S	P	D	T												
10^{-1}	(F)	144	53	138	21	144	53	138	19	144	53	138	19	144	53	138	19
10^{-2}	(F)	161	55	134	21	161	55	134	21	161	55	134	21	161	55	134	21
10^{-3}		97	32	66	11	145	44	96	17	145	44	96	17	145	44	96	17
10^{-4}		97	32	67	11	127	39	68	14	155	36	70	16	155	36	70	16
(c) $N = 2^{11} + 1$																	
rel \ abs		10^{-1}				10^{-2}				10^{-3}				10^{-4}			
		S	P	D	T												
10^{-1}	(F)	136	49	126	33	136	49	126	31	136	49	126	31	136	49	126	31
10^{-2}	(F)	154	54	135	34	154	54	135	35	154	54	135	35	154	54	135	35
10^{-3}		100	30	64	19	115	31	61	20	115	31	61	20	115	31	61	20
10^{-4}		101	30	65	19	133	35	66	24	160	35	71	27	160	35	71	27
(d) $N = 2^{12} + 1$																	
rel \ abs		10^{-1}				10^{-2}				10^{-3}				10^{-4}			
		S	P	D	T												
10^{-1}	(F)	138	59	147	94	138	59	147	96	138	59	147	91	138	59	147	90
10^{-2}	(F)	152	51	125	85	152	51	125	84	152	51	125	83	152	51	125	85
10^{-3}		102	31	62	47	115	31	61	56	115	31	61	51	115	31	61	50
10^{-4}		105	31	62	36	137	39	71	47	157	36	70	50	157	36	70	49

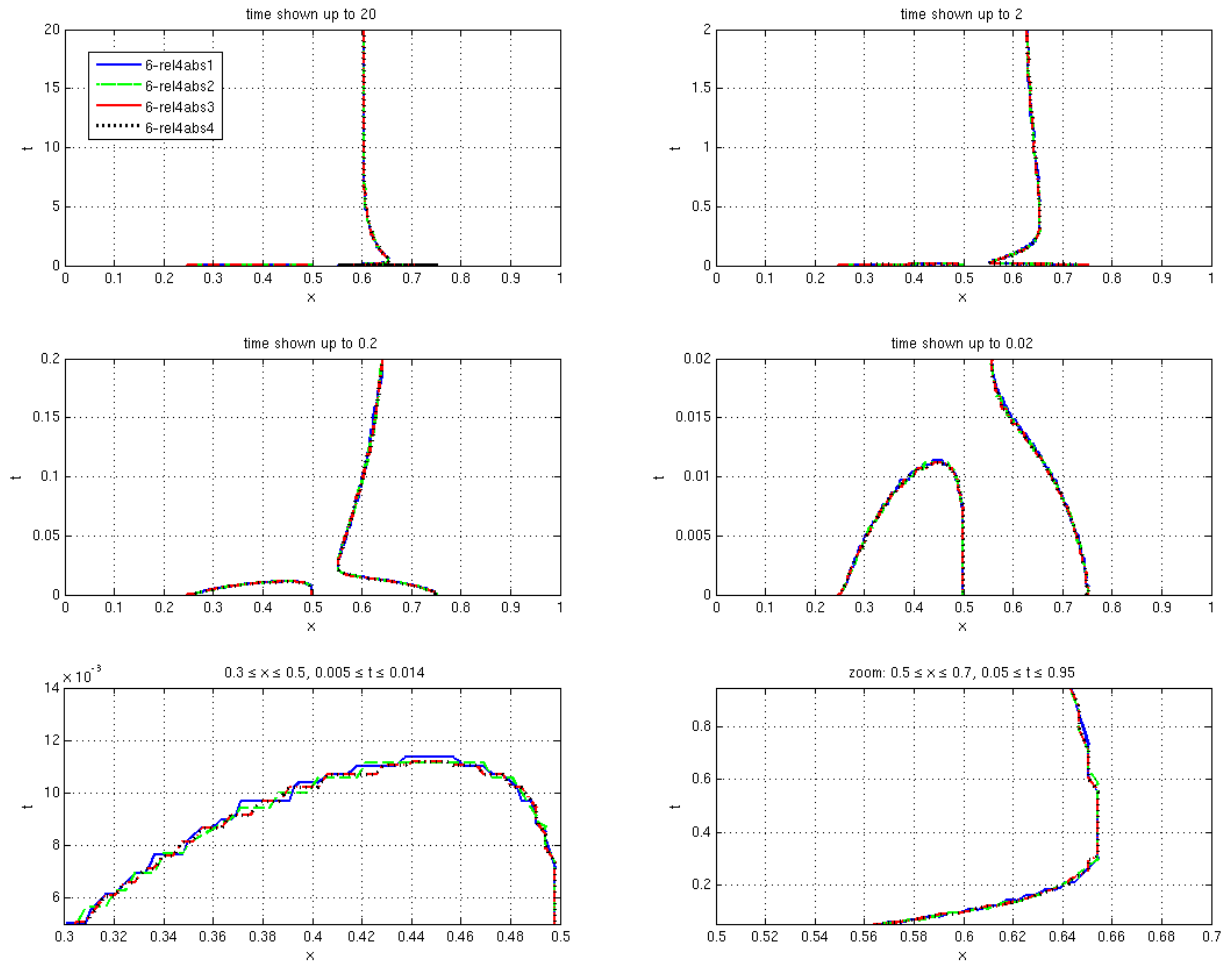


Figure 4: Simulation results of the reactant concentrations $u(x, t)$, $v(x, t)$ interface solutions for reaction coefficients $\lambda = 10^6$ with mesh size $N = 2^{10} + 1$ in the (x, t) -plane. The data corresponding to $\lambda = 10^6$ was collected with ODE relative tolerance of 10^{-4} and ODE absolute tolerances 10^{-1} , 10^{-2} , 10^{-3} and 10^{-4} . The top four plots overlay these cases for comparison in progressively decreasing time spans. The left bottom plot shows the movement of the left portion of the interface zoomed into $0.3 \leq x \leq 0.5$ and $0.005 \leq t \leq 0.014$. The right bottom plot shows the movement of the right portion of the interface zoomed into $0.5 \leq x \leq 0.7$ and $0.05 \leq t \leq 0.95$.

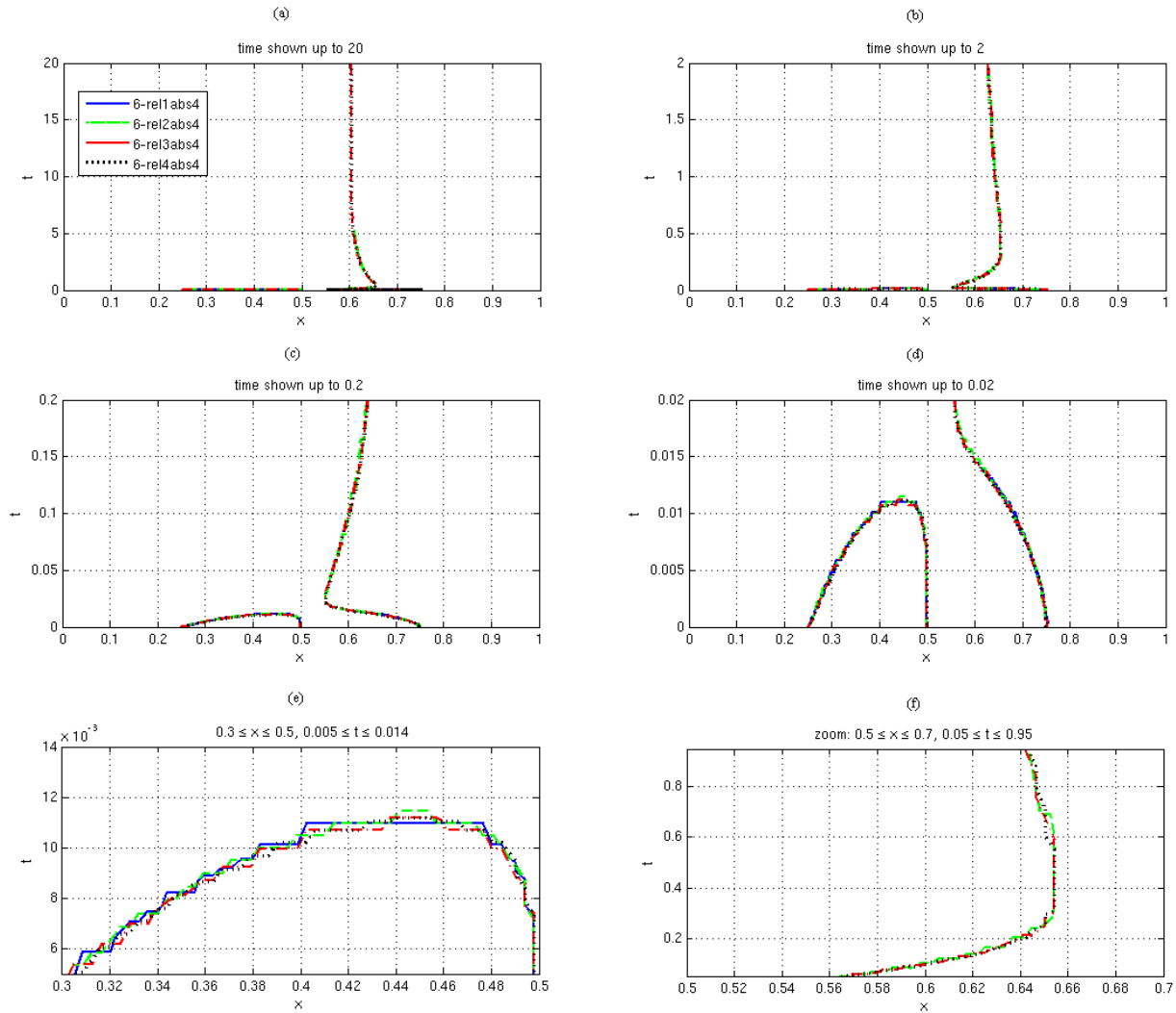


Figure 5: Simulation results of the reactant concentrations $u(x, t)$, $v(x, t)$ interface solutions for reaction coefficients $\lambda = 10^6$ with mesh size $N = 2^{10} + 1$ in the (x, t) -plane. The data corresponding to $\lambda = 10^6$ was collected with ODE absolute tolerance of 10^{-4} and ODE relative tolerances 10^{-1} , 10^{-2} , 10^{-3} and 10^{-4} . The top four plots overlay these cases for comparison in progressively decreasing time spans. The left bottom plot shows the movement of the left portion of the interface zoomed into $0.3 \leq x \leq 0.5$ and $0.005 \leq t \leq 0.014$. The right bottom plot shows the movement of the right portion of the interface zoomed into $0.5 \leq x \leq 0.7$ and $0.05 \leq t \leq 0.95$.

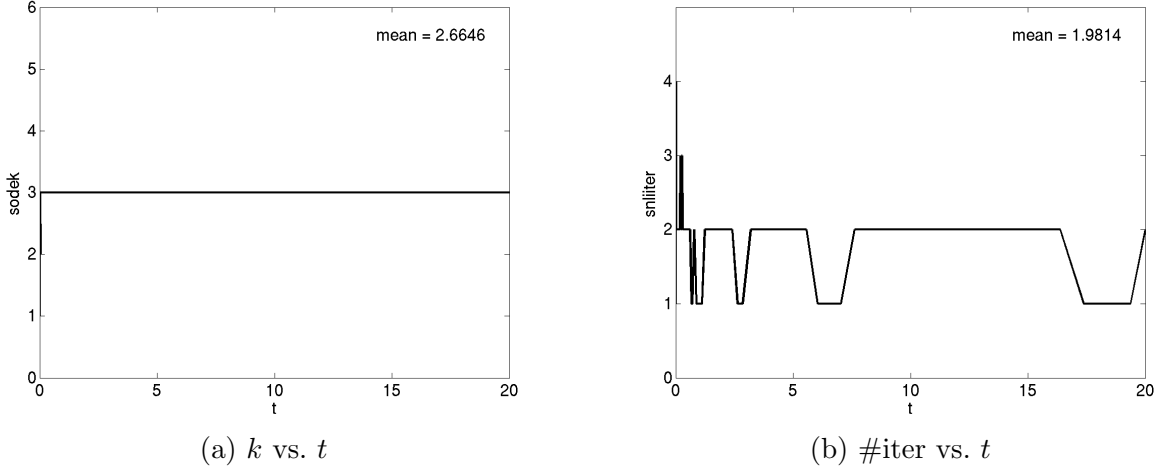


Figure 6: Numerical Differentiation Formulas (NDF k) method order and number of Newton iterations for $\lambda = 10^6$ with mesh size $N = 2^{10} + 1$. (a) NDF k method order k vs. t required during the computation. (b) Number of Newton iterations (#iter) vs. t required during the computation.

for each relative tolerance track closely with each other. Therefore, for the convergent cases, we see no significant change in accuracy.

Finally, Figure 6 shows the method order $1 \leq k \leq 5$ of the Numerical Differentiation Formulas (NDF k) in `ode15s` and the number of Newton iteration performance for $\lambda = 10^6$ with mesh size $N = 2^{10} + 1$. Figure 6 (a) plots the NDF k method order k vs. t reported by `ode15s` during the computation of the solution. Figure 6 (b) plots the number of Newton iterations (#iter) vs. t required during the computation of the solution. In Figure 6 (a) the (NDF k) method order is 3 most of the time during the computation and Figure 6 (b) shows the number of Newton iterations required to solve the non-linear system of equations at each time step is typically either 1 or 2 Newton steps.

5 Numerical Results for $\lambda = 10^9$

Table 2 reports the efficiency parameters for $\lambda = 10^9$ in the same manner as in Table 1. However, the solution fails to converge for any of the previous tolerances values. We suspect the higher reaction coefficient representing a wider differences in the slow and fast reaction processes leads to a stiffer model problem. Therefore, we re-ran our study with a the tighter set of tolerance values 10^{-2} , 10^{-4} , 10^{-6} and 10^{-8} for both absolute and relative tolerances with the findings reported in Table 3. The tighter set of tolerance values resulted in convergent solutions for absolute tolerances less than 10^{-2} and relative tolerances 10^{-6} and 10^{-8} .

Considering only the convergent cases in Table 3, we see the number of ODE steps, Jacobian evaluations, and LU decompositions remain roughly unchanged as we increase the mesh size N from $2^{10} + 1$ through $2^{12} + 1$. The number of Jacobian evaluations does however seem to tend to a stable value (approximately 352) as we tighten both the absolute and relative ODE tolerance values. The number of ODE steps S dramatically increases as we vary the absolute tolerance while keeping the relative tolerance at 10^{-8} . However, it is interesting to note that S varies little with absolute tolerance if the relative tolerance is kept at 10^{-6} . We also observe that the computation time T approximately doubles for every doubling of N . We note that the minimum computation time in Table 3 is 127 seconds for the $\lambda = 10^9$ cases with $N = 2^{10} + 1$, absolute tolerance 10^{-8} and relative tolerances 10^{-6} and 10^{-8} that were used for comparing the interface accuracy in Figure 3.

As in Section 4, we study the accuracy of the interface solutions for convergent cases but now using the tighter set of absolute and relative ODE tolerances mentioned above. In Figure 7 the relative tolerance is set constant to 10^{-8} for absolute tolerances 10^{-2} , 10^{-4} , 10^{-6} , and 10^{-8} . Similar to Section 4, we observe

Table 2: Table of `ode15s` efficiency statistics for $\lambda = 10^9$. The number of ODE steps (S), number of Jacobian evaluations (P), number of LU decompositions (D) and computation time (T) in seconds are reported across absolute (abs) and relative (rel) tolerances values for each mesh size N . The **(F)** in all entries in the (rel) column indicates failure of every combination of absolute and relative tolerance values in achieving successful completion.

(a) $N = 2^9 + 1$																
rel \ abs	10^{-1}				10^{-2}				10^{-3}				10^{-4}			
	S	P	D	T												
10^{-1} (F)	131	51	128	14	131	51	128	14	131	51	128	12	131	51	128	12
10^{-2} (F)	141	31	156	16	144	31	156	16	141	31	156	18	144	31	156	17
10^{-3} (F)	249	42	194	22	161	10	109	15	161	10	109	14	161	10	109	15
10^{-4} (F)	322	62	244	27	701	308	759	70	830	303	750	75	830	303	750	75
(b) $N = 2^{10} + 1$																
rel \ abs	10^{-1}				10^{-2}				10^{-3}				10^{-4}			
	S	P	D	T												
10^{-1} (F)	139	50	139	19	139	50	139	19	139	50	139	19	139	50	139	19
10^{-2} (F)	161	61	159	23	161	61	159	23	161	61	159	23	161	61	159	23
10^{-3} (F)	216	56	211	31	649	275	716	100	649	275	716	99	649	275	716	101
10^{-4} (F)	285	59	223	36	281	12	127	29	728	286	668	103	728	286	668	105
(c) $N = 2^{11} + 1$																
rel \ abs	10^{-1}				10^{-2}				10^{-3}				10^{-4}			
	S	P	D	T												
10^{-1} (F)	116	39	103	28	116	39	103	27	116	39	103	27	116	39	103	27
10^{-2} (F)	145	50	130	36	145	50	130	37	145	50	130	36	145	50	130	37
10^{-3} (F)	193	46	173	49	423	187	464	120	423	187	464	116	423	187	464	116
10^{-4} (F)	253	46	178	53	681	296	702	174	696	277	618	167	696	277	618	166
(d) $N = 2^{12} + 1$																
rel \ abs	10^{-1}				10^{-2}				10^{-3}				10^{-4}			
	S	P	D	T												
10^{-1} (F)	99	35	93	46	99	35	93	47	99	35	93	46	99	35	93	46
10^{-2} (F)	131	46	124	62	131	46	124	62	131	46	124	62	131	46	124	62
10^{-3} (F)	223	69	223	111	584	260	672	310	584	260	672	310	584	260	672	312
10^{-4} (F)	279	69	227	121	741	308	736	304	854	308	780	329	854	308	780	320

Table 3: Table of `ode15s` efficiency statistics for $\lambda = 10^9$ reporting the results of re-trials with tighter absolute and tighter relative tolerances than the values used for $\lambda = 10^6$. The number of ODE steps (S), number of Jacobian evaluations (P), number of LU decompositions (D) and computation time (T) in seconds are reported across absolute (abs) and relative (rel) tolerance values for each mesh size N . An **(F)** in the (rel) column indicates the relative tolerance results in failure across every absolute tolerance value. An **(F)** in a particular absolute tolerance box indicates the specific relative and absolute tolerance values resulting in unsuccessful completion.

(a) $N = 2^9 + 1$																
rel \ abs	10^{-2}				10^{-4}				10^{-6}				10^{-8}			
	S	P	D	T	S	P	D	T	S	P	D	T	S	P	D	T
10^{-2} (F)	144	31	156	25	144	31	156	20	144	31	156	22	144	31	156	20
10^{-4} (F)	701	308	759	91	830	303	750	95	830	303	750	101	830	303	750	99
10^{-6}	609	219	551	70 (F)	821	454	672	110	992	448	694	128	992	448	694	129
10^{-8}	554	133	363	56 (F)	813	455	671	113	1918	397	868	188	2701	382	992	238
(b) $N = 2^{10} + 1$																
rel \ abs	10^{-2}				10^{-4}				10^{-6}				10^{-8}			
	S	P	D	T	S	P	D	T	S	P	D	T	S	P	D	T
10^{-2} (F)	161	61	159	34	161	61	159	32	161	61	159	31	161	61	159	30
10^{-4} (F)	281	12	127	38	728	286	668	136	728	286	668	138	728	286	668	136
10^{-6}	534	12	155	63 (F)	643	452	570	149	830	399	514	126	830	399	514	127
10^{-8}	716	12	149	58 (F)	647	454	573	119	1639	370	600	178	2124	352	603	211
(c) $N = 2^{11} + 1$																
rel \ abs	10^{-2}				10^{-4}				10^{-6}				10^{-8}			
	S	P	D	T	S	P	D	T	S	P	D	T	S	P	D	T
10^{-2} (F)	145	50	130	49	145	50	130	48	145	50	130	52	145	50	130	49
10^{-4} (F)	681	296	702	233	696	277	618	217	696	277	618	219	696	277	618	220
10^{-6}	665	288	664	222 (F)	670	462	572	269	827	398	516	273	827	398	516	273
10^{-8}	665	288	664	222 (F)	676	463	574	273	1706	344	551	389	2056	353	572	441
(d) $N = 2^{12} + 1$																
rel \ abs	10^{-2}				10^{-4}				10^{-6}				10^{-8}			
	S	P	D	T	S	P	D	T	S	P	D	T	S	P	D	T
10^{-2} (F)	131	46	124	82	131	46	124	83	131	46	124	82	131	46	124	81
10^{-4} (F)	741	308	736	474	854	308	780	506	854	308	780	506	854	308	780	509
10^{-6}	572	297	609	397 (F)	696	433	540	525	827	393	511	528	827	393	511	527
10^{-8}	572	297	609	396 (F)	712	433	542	524	1802	356	550	770	2031	352	560	858

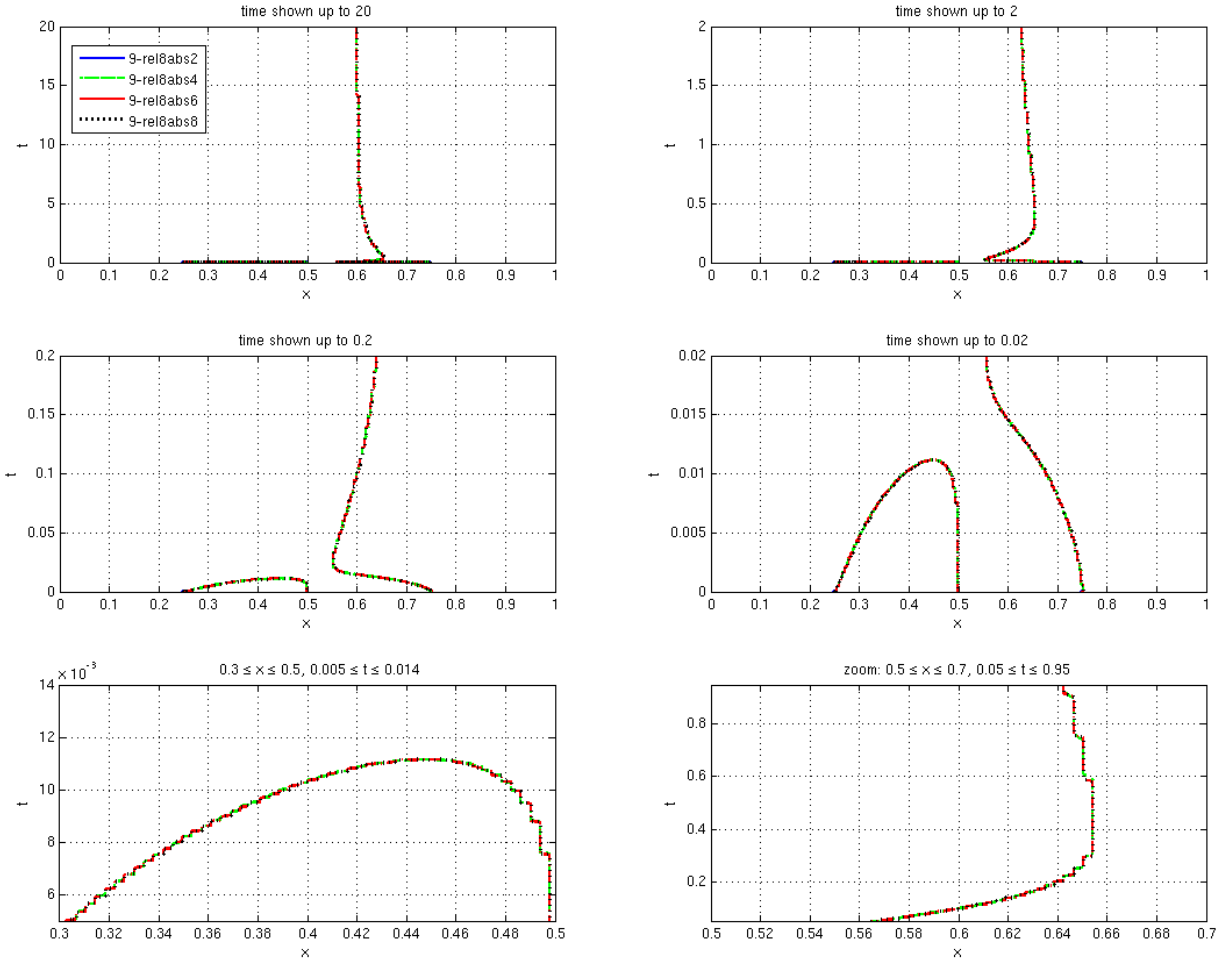


Figure 7: Simulation results of the concentration interface for the reaction coefficient $\lambda = 10^9$ in the (x, t) -plane. The top four plots overlay the results for comparison in progressively decreasing time spans. The left bottom plot shows the movement of the left portion of the interface zoomed into $0.3 \leq x \leq 0.5$ and $0.005 \leq t \leq 0.014$. The right bottom plot shows the movement of the right portion of the interface zoomed into $0.5 \leq x \leq 0.7$ and $0.05 \leq t \leq 0.95$. A mesh size of $N = 2^{10} + 1$ is used. The data shown used an relative ODE tolerance 10^{-8} and absolute ODE tolerances 10^{-2} , 10^{-4} , 10^{-6} , and 10^{-8} .

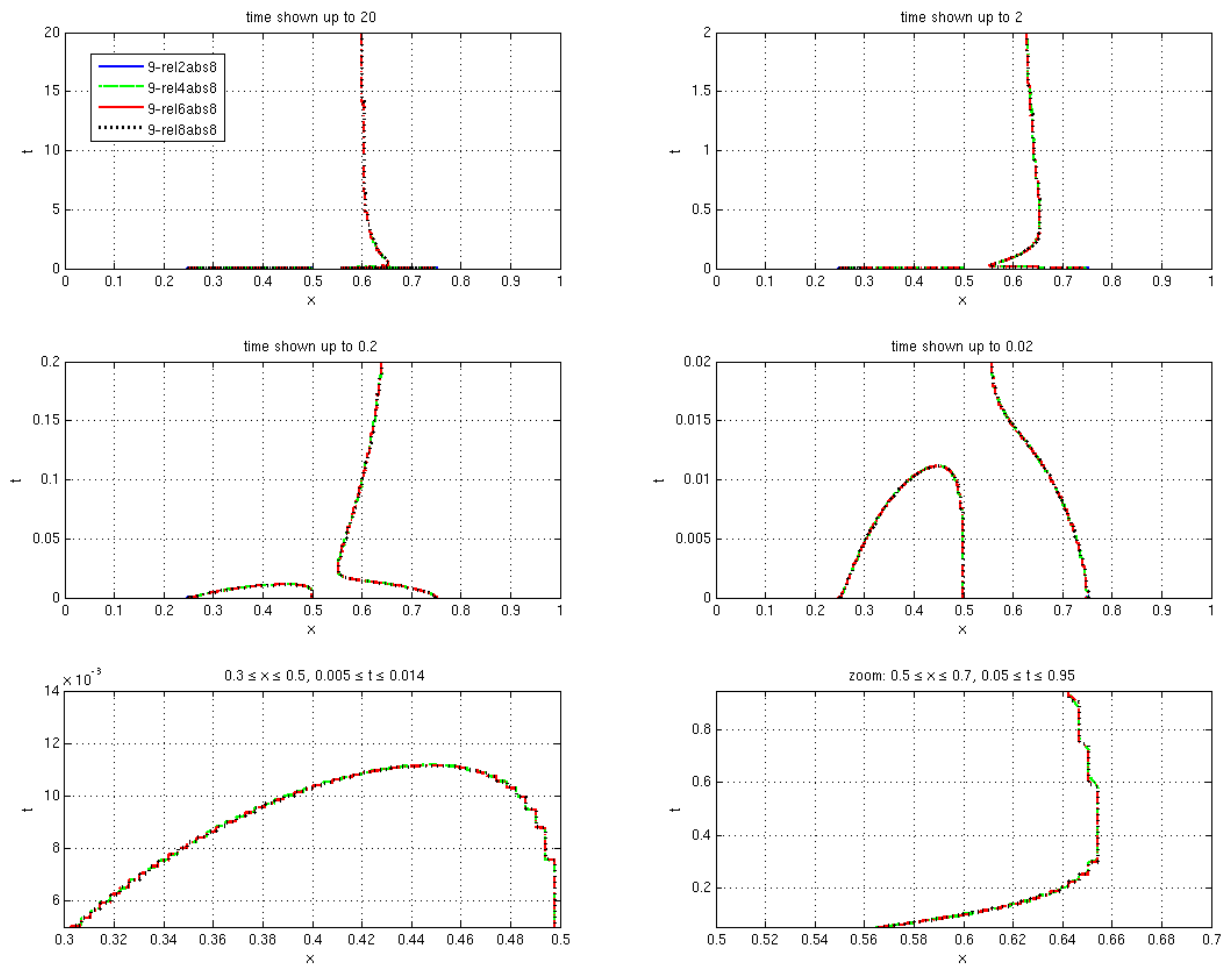


Figure 8: Simulation results of the concentration interface for the reaction coefficient $\lambda = 10^9$ in the (x, t) -plane. The top four plots overlay the results for comparison in progressively decreasing time spans. The left bottom plot shows the movement of the left portion of the interface zoomed into $0.3 \leq x \leq 0.5$ and $0.005 \leq t \leq 0.014$. The right bottom plot shows the movement of the right portion of the interface zoomed into $0.5 \leq x \leq 0.7$ and $0.05 \leq t \leq 0.95$. A mesh size of $N = 2^{10} + 1$ is used. The data shown used an absolute ODE tolerance 10^{-8} and relative ODE tolerances 10^{-2} , 10^{-4} , 10^{-6} , and 10^{-8} .

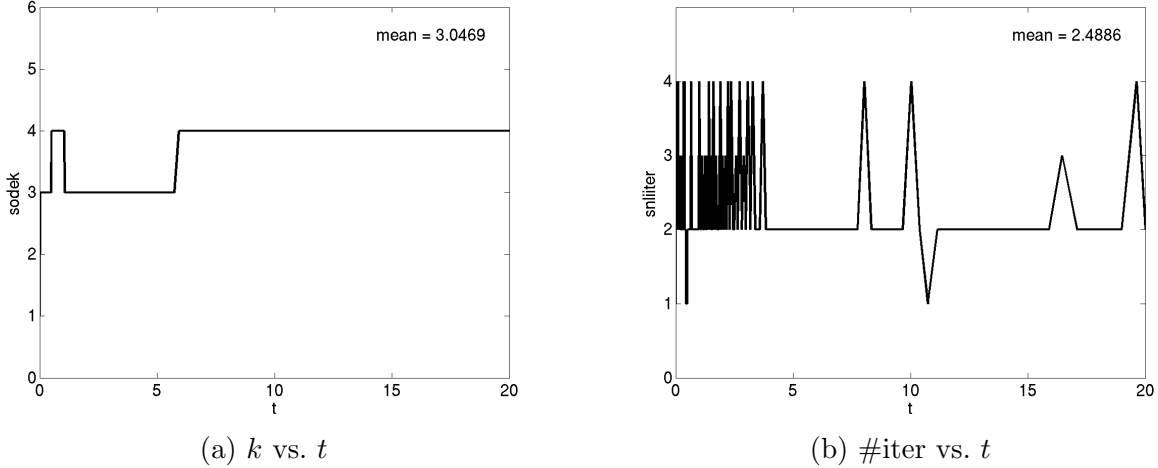


Figure 9: Numerical Differentiation Formulas (NDFk) method order and number of Newton iterations for $\lambda = 10^9$ with mesh size $N = 2^{10} + 1$. (a) NDFk method order k vs. t required during the computation. (b) Number of Newton iterations (#iter) vs. t required during the computation.

that the interface solutions overlay closely with each other as we tighten the absolute tolerance showing no significant differences in accuracy. Similarly, in Figure 8 where the absolute tolerance is set to a constant 10^{-8} and for the convergent relative tolerances 10^{-6} and 10^{-8} , we observe little difference in accuracy as the relative tolerance is tightened. We conclude tightening either absolute or relative ODE tolerances for $\lambda = 10^9$ gives essentially the same accuracy.

Finally, Figure 9 shows the method order $1 \leq k \leq 5$ of the Numerical Differentiation Formulas (NDFk) in `ode15s` and the number of Newton iteration performance for $\lambda = 10^9$ with mesh size $N = 2^{10} + 1$ analogous to Figure 6 of Section 4. Figure 9 (a) shows the (NDFk) method order is 4 for a predominant portion of the computation time compared to 3 for the $\lambda = 10^6$ case. Moreover, Figure 9 (b) shows the number of Newton iterations at early time steps varies between 2, 3 and 4 while spending a significant amount of time at 4 until settling predominantly at 2. Recall, the required number of Newton iterations cited for $\lambda = 10^6$ in the last section is typically 1 or 2 throughout the entire time span. We suspect the notable increase in the number of Newton steps for $\lambda = 10^9$ at the beginning of the time span $t \in [0, 4]$ compared to Figure 6 (b) for $\lambda = 10^6$ is the result of a greater stiffness in the model problem requiring smaller time steps to compute a convergent solution.

A Finite Differences for the Interface Problem

In this appendix, we present some details of how the interface problem (2.1)–(2.3) is discretized by the finite difference method within a method of lines approach to obtain a system of ODEs. This explains how the ODE system arises without a mass matrix in (3.1) and how we have handled the Dirichlet boundary conditions given for u and v in (2.2). We define a uniform spatial mesh with N nodes and spacing $\Delta x = 1/(N - 1)$ by $x_j = (j - 1) \Delta x$ for $j = 1, \dots, N$, and let $u_j(t)$, $v_j(t)$, $w_j(t)$ denote approximations to $u(x_j, t)$, $v(x_j, t)$, $w(x_j, t)$, respectively.

The boundary conditions for the first and second species u and v have mixed Dirichlet and Neumann boundary conditions, while the third one w has Neumann boundary conditions at both endpoints. Thus, for clarity of presentation, we derive first the semi-discretization for the third species that satisfies $w_t = w_{xx} + \lambda uv - uw$ in (2.1) together with homogeneous Neumann boundary conditions in (2.2). Approximating the spatial derivative by a second-order centered difference approximation at interior nodes yields

$$\frac{dw_j}{dt} = \frac{w_{j-1} - 2w_j + w_{j+1}}{\Delta x^2} + \lambda u_j v_j - u_j w_j, \quad j = 2, \dots, N - 1. \quad (\text{A.1})$$

This yields $N - 2$ ODEs for the N unknowns w_j ; we obtain the remaining 2 ODEs from the boundary conditions. First consider the boundary at $x = x_1 = 0$. To ensure that those conditions are also second-order accurate, we introduce a ghostpoint $x_0 = x_1 - \Delta x$ and evaluate the PDE for $w(x, t)$ on the boundary to find

$$\frac{dw_1}{dt} = \frac{w_0 - 2w_1 + w_2}{\Delta x^2} + \lambda u_1 v_1 - u_1 w_1. \quad (\text{A.2})$$

The centered difference approximation to the boundary condition for w at $x = 0$ in (2.2) is $(w_2 - w_0)/(2\Delta x) = 0$ and gives the condition $w_0 = w_2$, which is used in (A.2) to eliminate the ghostvalue w_0 to yield

$$\frac{dw_1}{dt} = \frac{-2w_1 + 2w_2}{\Delta x^2} + \lambda u_1 v_1 - u_1 w_1. \quad (\text{A.3})$$

Use of the same techniques yields also

$$\frac{dw_N}{dt} = \frac{2w_{N-1} - 2w_N}{\Delta x^2} + \lambda u_N v_N - u_N w_N. \quad (\text{A.4})$$

We now organize the equations in system form for the (column) vector of unknowns $W := [w_1, \dots, w_N]^T$ as

$$\frac{dW}{dt} = -K^{(w)} W + r^{(w)}(U, V, W), \quad 0 < t \leq t_{\text{fin}}, \quad W(0) = W_{\text{ini}}, \quad (\text{A.5})$$

where we also define the vectors $U := [u_1, \dots, u_N]^T$ and $V := [v_1, \dots, v_N]^T$. Here, the constant stiffness matrix $K^{(w)} \in \mathbb{R}^{N \times N}$ and the vector function $r^{(w)} \in \mathbb{R}^N$ are defined as

$$K^{(w)} = \frac{1}{\Delta x^2} \begin{bmatrix} 2 & -2 & & & & \\ -1 & 2 & -1 & & & \\ & & \ddots & \ddots & \ddots & \\ & & & -1 & 2 & -1 \\ & & & & -2 & 2 \end{bmatrix}, \quad r^{(w)} = \begin{bmatrix} \lambda u_1 v_1 - u_1 w_1 \\ \lambda u_2 v_2 - u_2 w_2 \\ \vdots \\ \lambda u_{N-1} v_{N-1} - u_{N-1} w_{N-1} \\ \lambda u_N v_N - u_N w_N \end{bmatrix}.$$

We note that we have allowed the function $r^{(w)}(U, V, W)$ in (A.5) to depend on all three vectors of unknowns for generality. Also, we note that $K^{(w)}$ has non-negative diagonal and non-positive off-diagonal entries, but is not symmetric.

For the discretization of the u equation in (2.1), the discretization of the PDE and the Neumann boundary condition $u_x = 0$ at $x = 1$ in (2.2) proceeds analogously to the one for the w equation. To implement the Dirichlet boundary condition $u = \alpha$ at $x = 0$ in (2.2), we formally introduce the ODE

$$\frac{du_1}{dt} = 0, \quad u_1(0) = \alpha. \quad (\text{A.6})$$

This equation is used to replace the first row in all terms in the ODE system appropriately. Notice that we are using the consistency of boundary and initial data here as well as the time independence of the Dirichlet boundary conditions. Finally, we organize the equations in system form for the vector U as

$$\frac{dU}{dt} = -K^{(u)} U + r^{(u)}(U, V, W), \quad 0 < t \leq t_{\text{fin}}, \quad U(0) = U_{\text{ini}}, \quad (\text{A.7})$$

with

$$K^{(u)} = \frac{1}{\Delta x^2} \begin{bmatrix} 0 & 0 & & & & \\ -1 & 2 & -1 & & & \\ & & \ddots & \ddots & \ddots & \\ & & & -1 & 2 & -1 \\ & & & & -2 & 2 \end{bmatrix}, \quad r^{(u)} = \begin{bmatrix} 0 \\ -\lambda u_2 v_2 - u_2 w_2 \\ \vdots \\ -\lambda u_{N-1} v_{N-1} - u_{N-1} w_{N-1} \\ -\lambda u_N v_N - u_N w_N \end{bmatrix}.$$

